Inhibition of HDAC6 alleviates cancer-induced bone pain by reducing the activation of NLRP3 inflammasome

YIN-DI HU[1*], ZHAO-DI WANG[1*], YUAN-FEN YUE[2*], DAI LI[3], SHU-QING ZHEN[4], JIE-QIONG DING[3], WEI MENG[3], HAI-LI ZHU[3], MIN XIE[3*] and LING LIU[3*]

[1]School of Pharmacy, Hubei University of Science and Technology, Xianning, Hubei 437100; [2]Xianning Central Hospital, First Affiliated Hospital of Hubei University of Science and Technology, Xianning, Hubei 437199; [3]Hubei Key Laboratory of Diabetes and Angiopathy, School of Basic Medical Sciences, Xianning Medical College, Hubei University of Science and Technology, Xianning, Hubei 437100; [4]Matang Hospital of Traditional Chinese Medicine, Xianning, Hubei 437000, P.R. China

Received June 15, 2023; Accepted October 30, 2023

DOI: 10.3892/ijmm.2023.5328

Abstract. Cancer-induced bone pain (CIBP) is characterized as moderate to severe pain that negatively affects the daily functional status and quality of life of patients. When cancer cells metastasize and grow in bone marrow, this activates neuroinflammation in the spinal cord, which plays a vital role in the generation and persistence of chronic pain. In the present study, a model of CIBP was constructed by inoculating of MRMT-1 rat breast carcinoma cells into the medullary cavity of the tibia in male Sprague-Dawley rats. Following two weeks of surgery, CIBP rats exhibited damaged bone structure, increased pain sensitivity and impaired motor coordination. Neuroinflammation was activated in the spinal cords of CIBP rats, presenting with extensive leukocyte filtration, upregulated cytokine levels and activated astrocytes. Histone deacetylase 6 (HDAC6) works as a therapeutic target for chronic pain. The intrathecal injection of the HDAC6 inhibitor tubastatin A (TSA) in the lumbar spinal cord resulted in decreased spinal inflammatory cytokine production, suppressed spinal astrocytes activation and reduced NOD-like receptor pyrin domain containing 3 (NLRP3) inflammasome activity. Consequently, this effect alleviated spontaneous pain and mechanical hyperalgesia and recovered motor coordination in CIBP rats. It was demonstrated by immunoprecipitation assay that TSA treatment reduced the interaction between HDAC6 and NLRP3. Cell research on C6 rat glioma cells served to verify that TSA treatment reduced HDAC6 and NLRP3 expression. In summary, the findings of present study indicated that TSA treatment alleviated cancer-induced bone pain through the inhibition of HDAC6/NLRP3 inflammasome signaling in the spinal cord.

Correspondence to: Dr Min Xie or Dr Ling Liu, Hubei Key Laboratory of Diabetes and Angiopathy, School of Basic Medical Sciences, Xianning Medical College, Hubei University of Science and Technology, 88 Xiangning Road, Xianning, Hubei 437100, P.R. China
E-mail: xiemin2020a@163.com
E-mail: liuling0306@163.com

*Contributed equally

Key words: cancer induced bone pain, neuroinflammation, NOD-like receptor pyrin domain containing 3 inflammasome, histone deacetylase 6

Introduction

Cancer pain is the most frequently occurring and problematic symptom of cancer and is experienced by 66.4% of patients with advanced cancer (1). Bones are a particularly common site for cancer metastases. The bone metastasis incidence is ~30-75% with breast cancer and prostate cancer (2). Bone metastasis leads to hypercalcemia, pathological skeletal fractures, compression of the spinal cord and pain (3). Cancer-induced bone pain (CIBP) is characterized as moderate to severe pain and is a combination of background, spontaneous and incidental pain that persists for years (4). According to the World Health Organization approach to cancer pain treatment, a three-step ladder provides guidelines for patients with cancer pain, including nonopioid pain medications and lower or higher potency opioids for mild to moderate or moderate to severe pain (5). However, ~30% of patients were dissatisfied with the treatment. (6) Depending on the advanced treatment and increased diagnoses, almost half of cancer patients live for longer than 10 years (7). As a result, this means that an increased number of patients with cancer are suffering from uncontrolled pain. Elucidating the pathogenesis of CIBP would be helpful for the development of novel therapies for pathological pain.

Spinal inflammation plays a major role in chronic pain. When cancer cells metastasize and grow in bone marrow, bone structure becomes impaired, inflammatory infiltration in the bone is increased and the nociceptive signals are stimulated (8). Nociceptive signals enter the spinal cord serve to activate neuroinflammation, which is characterized by leukocyte infiltration, glial activation and the release of pro-inflammatory cytokines and chemokines (9,10). Elevated levels of neuroinflammation have been observed in patients with chronic pain,

including lumbar radiculopathy and pain-positive human immunodeficiency virus (11). Neuroinflammation in the spinal cord is also activated in rodent models of several types of chronic pain, including inflammation pain, neuropathic pain, chemotherapy pain and bone cancer pain (12,13). The NOD-like receptor pyrin domain-containing 3 (NLRP3) inflammasome mediates caspase-1 activation and proinflammatory cytokine IL-1β secretion and participates in chronic pain (14). Activated NLRP3 recruits the apoptosis-associated speck-like protein that contains a CARD (ASC) and caspase-1 as a means of forming NLRP3 inflammasome (15). The activated caspase-1 cleaves IL-1β to maturation and secretion (16). Increased NLRP3 and IL-1β expressions are found in the blood of patients who suffer from fibromyalgia, which is a type of chronic pain (17). MCC950 is a specific small molecular inhibitor of NLRP3 inflammasome treatment that reduces NLRP3, ASC, caspase-1 and IL-1β expression levels to basal levels in the spinal cord and attenuates mechanical allodynia in the rodent models of cancer-induced bone pain and oxaliplatin-induced peripheral neuropathy (18-20). Therefore, inhibiting NLRP inflammasome-mediated neuroinflammation in the spinal cord is a potential therapeutic strategy for pathological pain.

Histone deacetylase (HDAC) 6 is a cytoplasmic class II HDAC that is considered to be a potential therapeutic target for chronic pain (21). The dysregulation of HDAC6 has been implicated in peripheral neuropathy and neuropathic pain (22). HDAC6 inhibitor SW-100 treatment restores α-tubulin acetylation loss in sciatic nerve tissue while also alleviating mechanical allodynia and hyperalgesia in the peripheral neuropathy mouse model of Charcot-Marie-Tooth disease (23). Cisplatin-induced mechanical allodynia and spontaneous pain are reversed in chemotherapy-induced peripheral neuropathy model mice by HDAC6 inhibitor ACY-1083 (24). The genetic deletion of HDAC6 serves to protect against cisplatin-induced mechanical allodynia (25). HDAC6 plays a crucial role at the intersection of pathogenic pathways, which includes the cellular responses to protein stress, organelle damage and neuroinflammatory signaling (26). HDAC6 functions as a dynein adapter and facilitates the retrograde transporting of NLRP3 inflammasome for activation (27). Research on animal models linked to inflammation has indicated that HDAC6 inhibition serves to improve neuropathies through the downregulation of NLRP3 inflammasome activation (28). The application of HDAC6 degrader attenuates the activation of NLRP3 inflammasome in lipopolysaccharide-induced mice (29). The inhibition of HDAC6 decreases NLRP3 and IL-1β expressions while also suppressing nicotine-induced pyroptosis in atherosclerosis model mice (30). The inhibition of HDAC6 by tubastatin (TSA) attenuates NLRP3 expression and the maturation of caspase-1 and IL-1β in Parkinson's disease model mice (31). Accordingly, targeting HDAC6 is promising for the management of chronic pain and neuroinflammation.

In the present study, HDAC6 inhibitor TSA was injected into the spinal cords of CIBP rats as a means of investigating the effect of HDAC6 on cancer pain and changes in behaviors and spinal inflammation were subsequently detected. The aim of present study was to clarify the effect of HDAC6 inhibition has on cancer pain alleviation and providing an analgesic target for the management of cancer pain.

Materials and methods

Antibodies and reagents. The following antibodies were used in the cell and tissue analysis: Anti-glial fibrillary acidic protein (GFAP; cat. no. A19058), anti-complement factor B (CFB) (cat. no. A13243), anti-NLRP3 (cat. no. A12694), anti-NF-κB (cat. no. A19653), anti-caspase-1 (cat. no. A16792), anti-TNF-α (cat. no. A11534) and anti-HDAC6 (cat. no. A1732) were purchased from ABclonal Biotech Co., Ltd.; anti-IL-1β (cat. no. AF5103), anti-C3 (cat. no. DF13224), anti-GFAP (cat. no. BF8023), anti-NLRP3 (cat. no. BF8029) and anti-β-actin (cat. no. AF7018), were purchased from Affinity Biosciences; and anti-pSer22-HDAC6 (cat. no. YP0922), which was purchased from ImmunoWay Biotechnology Company. The secondary antibodies that were used for western blotting were HRP Goat anti-rabbit IgG (H+L; cat. no. AS014) and HRP Goat Anti-Mouse IgG (H+L; cat. no. AS003), which were purchased from ABclonal Biotech Co., Ltd. The secondary antibodies that were used for immunofluorescence analysis were Alexa Fluor 555-labeled Donkey Anti-Rabbit IgG (H+L; cat. no. A0453) and Alexa Fluor 488-labeled Goat Anti-Rabbit IgG (H+L; cat. no. A0423), which were purchased from Beyotime Institute of Biotechnology. Tubastatin A (cat. no. S8049) was purchased from Selleck Chemicals. Hematoxylin and eosin (H&E) staining solution (cat. no. BL735B), phosphate buffer solution (cat. no. BL550A), 4% paraformaldehyde (PFA; cat. no. BL539A), 0.3% Triton X-100 (cat. no. BL935A) and ECL detection reagent (cat. no. BL520A) were all purchased from Biosharp Life Sciences. RPMI 1640 medium (cat. no. 11875119), fetal bovine serum (FBS; cat. no. 10091148), 50 U/ml penicillin and 50 μg/ml streptomycin (cat. no. 15140122), Hank's balance salt solution (HBSS; cat. no. 14170146) and DMEM medium (cat. no. 11320033) were all purchased from Gibco (Thermo Fisher Scientific, Inc.). IL-1β (cat. no. P5106; 10 μg), immunofluorescence blocking solution (cat. no. P0102), Hoechst 33342 (cat. no. C1027), RIPA lysis buffer (cat. no. P0013B), Protease inhibitors cocktail (cat. no. P1005), BCA protein assay kit (cat. no. BL521A), QuickBlock Blocking Buffer for Western Blot (cat. no. P0252; 500ml) and protein G agarose (cat. no. P2009) were all purchased from Beyotime Institute of Biotechnology. The commercial products HDAC6 short interfering (si) RNA (sc-35544), siRNA Transfection Medium (sc-36868), siRNA Transfection Reagent (sc-29528) and control siRNA (sc-37007) were both purchased from Santa Cruz Biotechnology, Inc.

Animals. A total of 27 male Sprague-Dawley rats that weighed 160-200 g (6-8 weeks) were purchased from Hubei Province Experimental Animal Center. All the rats were housed with *ad libitum* access to water and food in a 12-h light/dark cycle at a stable environment temperature of 22-24˚C and humidity of 55-58%. All procedures were conducted in accordance with the Chinese National Guidelines for the ethical review of animal welfare (GB/T 35892-2018, https://std.samr.gov.cn/gb/search/gbDetailed?id=71F772D8283AD3A7E05397BE0A0AB82A) and they were approved by the Ethics Committee

of Hubei University of Science and Technology (approval number 2020-01-900). The rats were allowed to acclimatize to their environment for five days before the experiments started. The 27 rats were divided at random into the three following groups: Sham-operated (sham) group, CIBP group and CIBP + TSA group; there were nine rats in each group.

Cell culture and treatment. MRMT-1 rat cells (cat. no. RCB2860; Jennio Biotech Co, Ltd.) were cultured in RPMI 1640 medium supplemented with 10% fetal bovine serum, 50 U/ml penicillin and 50 μg/ml streptomycin in a humidified incubator that contained 5% CO_2 at 37˚C. MRMT-1 cells were collected and the pellet was resuspended in Hank's balance salt solution (HBSS) for inoculation. Rat glioma cells (C6; cat. no. CBP60888; Jennio Biotech Co., Ltd.) and U-87 MG cells (cat. no. HTB-14; Jennio Biotech Co., Ltd.) were cultured in and DMEM medium with 10% fetal bovine serum, 50 U/ml penicillin and 50 μg/ml streptomycin at 37˚C with 5% CO_2. C6 and U-87 MG cells were cultured in the 24-well plate with sterilized coverslips, stimulated with IL-1β (5 ng/ml) for 30 min and incubated with 1 μM TSA at 37˚C for 24 h for immunofluorescence assay. For western blot analysis, U-87 cells were treated with MCC950 (1 μM) or TSA (1 μM) for 24 h. Following 24 h of incubation, the whole-cell extracts were collected for biochemical analyses.

Establishment of the CIBP rat model and TSA administration. In order to establish the rat model of cancer-induced bone pain, centrifugation at 25˚C (845 x g; 2 min) was used to collect MRMT-1 rat mammary gland carcinoma cells from the cell suspension. The pellet was then resuspended in HBSS and kept on ice until use. The rats were anaesthetized with pentobarbital sodium (50 mg/kg) by intraperitoneal injection for inoculation. Once the left hind limb had been disinfected with 75% ethanol and shaved, $5.0x10^5$ MRMT-1 cells in HBSS were slowly injected into the intramedullary space of the left tibia bones of the CIBP and CIBP + TSA rats using a 50 μl Hamilton microsyringe. After the injection, the syringe remained in the injection site for an additional minute as a means of preventing tumor cells leakages. The injection site was sealed using bone wax once the syringe had been removed (32). The sham group rats were injected with an equivalent volume of the vehicle (HBSS) into the cavity. Following 14 days of inoculation, an intrathecal injection was administered with a 25-μl microsyringe, which was inserted into the intervertebral space of the rats between the L5 and L6 vertebrae. The HDAC6 inhibitor TSA was dissolved before use. The TSA dosage used in the present study was determined based on published research (33). The CIBP + TSA group rats were intrathecally injected with 10 μl TSA (1 mg/kg). The sham and CIBP group rats received an intrathecal injection of the same volume of the vehicle (10 μl).

Flinching number analysis. The rats were habituated for a minimum of 30 min before behavioral experiments were conducted. For the spontaneous pain test, the number of spontaneous flinches was recorded and counted for 5 min. This was repeated three times (34).

Paw withdrawal threshold (PWT) test. von Frey filaments, ranging 0.4-26 g (Stoelting Co.) were used for applying mechanical stimuli to the left hind paw. The 50% PWT was determined using Chaplan's up-down method (35). The filaments were pressed perpendicularly against the plantar surfaces until the filaments were bent and brisk withdrawal was considered to be a positive response. In the case of a positive response occurring, the von Frey filament with the next lower force was applied and in the case of a negative response occurring, the filament with the next higher force was applied. The pattern of positive and negative withdrawal responses was then converted to 50% PWT.

Rotarod test. An accelerating rotarod (ZS-RDM; Zhongshi Dichuang Technology Development) was used for assessing motor coordination and the balance of animals. For three days prior to the experiments, the rats were trained at a fixed speed of 4 revolutions/min for 10 min, which was repeated three times at 10-min intervals. At the start of the experiment, rotation speed was set at a fixed value of 10 revolutions/min for 10 sec, accelerated for 10 sec to a working speed of 20 revolutions/min for 30 sec and then accelerated again for 10 sec. This movement was continuously carried out for 10 min. The experiments were repeated three times with intervals of 10 min and the latency to fall of rats was recorded (36).

Bone X-ray and histological analysis. After the behavioral tests were performed, five rats from each group were sacrificed using an overdose of pentobarbital sodium (150 mg/kg) that was administered by intraperitoneal injection. For bone X-ray assay, legs were placed on X-ray film and exposed to an X-ray source and the roentgenography of the tibia was performed. For histological analysis, tibias were harvested, fixed in 4% PFA and decalcified in 10% decalcification solution. The decalcified bones were then rinsed, dehydrated, embedded in paraffin and sectioned into 4 μm sections using a microtome (cat. no. RM 2165; Leica Microsystems GmbH). The sections were deparaffinized, rehydrated and H&E staining was conducted in accordance with standard procedures. The sections were stained with hematoxylin solution for 3 min and then washed using tap water for 10 sec. The sections were stained with eosin for 3 min and then washed using tap water for 10 sec. The dehydration and clearing treatment were conducted by putting the sections into a series of ethanol (100, 90 and 70%, each for 10 min) and xylene (5 min, twice). The temperature was 25˚C for all procedures. The stained sections were observed through a fluorescence microscope at x60 magnification (Olympus IX73; Olympus Corporation) (37). The similar cell density and the state of three fields in each group were examined.

Spinal cord histology. Following the behavioral tests, five rats from each group were deeply anesthetized using 60 mg/kg sodium pentobarbital administered by intraperitoneal injection and perfused with 0.9% NaCl, followed by 4% PFA. Following the completion of perfusion, the spinal cords were removed, post-fixed in 4% PFA, embedded in paraffin as above and cut into 4 μm sections using a microtome. The sections were stained using the standard H&E method as aforementioned. H&E images were analyzed using ImageJ v1.51j8

software (National Institutes of Health). The scoring criteria of inflammation cell infiltration was as follows: 0 (normal); 1 (lymphocyte infiltration around meninges and blood vessels); 2 (1-10 lymphocytes in a field); 3 (11-100 lymphocytes in a field); and 4 (>100 lymphocytes in a field) (38).

Immunofluorescence assay. Following the completion of perfusion, the spinal cords were removed, post-fixed in 4% PFA, embedded in paraffin as above and cut into 4 μm sections using a microtome. The spinal cord sections were deparaffinized, incubated in 3% H_2O_2 for 10 min at 25˚C to quench endogenous peroxidase or biotin activity, blocked with immunofluorescence blocking solution at 25˚C for 60 min, incubated with primary antibodies at 4˚C for 24 h and secondary antibodies at 25˚C for 60 min, mounted with antifade mounting medium and observed through a fluorescence microscope (Olympus IX73; Olympus Corporation). The intensity was analyzed using ImageJ v1.48 software (National Institutes of Health).

After treatment, the cells were rinsed with phosphate buffer solution, fixed with 4% PFA, permeabilized with 0.5% Triton X-100, blocked with immunofluorescence blocking solution for 60 min at 25˚C, incubated with primary antibodies at 4˚C for 24 h and secondary antibodies at 25˚C for 60 min, counterstained with Hoechst 33342 (1 μg/ml) for 15 min at 25˚C, mounted with antifade mounting medium and observed via fluorescence microscopy (Olympus IX73; Olympus Corporation) for cell research. The intensity was analyzed using ImageJ v1.48 software (National Institutes of Health).

Western blot analysis. After the behavioral tests were completed, another five rats from each group were sacrificed with an overdose of pentobarbital sodium (150 mg/kg), which was administered by intraperitoneal injection. The spinal cord tissues were collected and homogenized in ice-cold RIPA lysis buffer that contained a cocktail of protease inhibitors. After being centrifugated at 13,523 x g at 4˚C for 15 min, the supernatant was used for western blotting. Protein concentration was determined using a BCA protein assay kit. The supernatant was collected, the protein samples were loaded at 30 μg per lane and separated by 8-12% SDS-PAGE, then transferred to PVDF membranes. The membranes were blocked using QuickBlock blocking buffer for western blot for 15 min at 25˚C and incubated with primary antibodies for 24 h at 4˚C. The membranes were rinsed and incubated with secondary antibodies for 60 min at 25˚C. The protein bands were visualized using ECL detection reagent and detected with an iBright 1500 instrument (Invitrogen). The bands were analyzed using ImageJ v1.48 software (National Institutes of Health) and β-actin was used as a loading control.

Following siRNA or drug treatment, the cells were lysed in ice-cold RIPA lysis buffer that was supplemented with the protease inhibitors for cell research. The subsequent procedures were the same as those for tissues.

Immunoprecipitation. The spinal cords were collected and homogenized in ice-cold RIPA lysis buffer that contained a cocktail of protease inhibitors. After being centrifugated at 13,523 x g for 20 min at 4˚C, the supernatant was collected as a protein sample (50 μl) and the protein G agarose (5 μl) was added and incubated at 4˚C for 60 min with rotation. The samples were then centrifugated at 13,523 x g for 15 min at 4˚C and the supernatants were transferred to fresh tubes. The primary antibodies (anti-NLRP3 and anti-HDAC6, 1:100) were then added and incubated at 4˚C for 24 h. This was followed by the addition of protein G agarose (10 μl) for capturing immune complexes at 4˚C with rotation. After being centrifugated at 13,523 x g for 1 min at 4˚C, the pellets were washed in ice-cold PBS (cat. no. C0221A, Beyotime). They were then centrifugated at 13,523 x g for 2 min at 4˚C and the supernatant was collected. Protein complexes were analyzed using immunoblot analysis and the primary antibodies were anti-HDAC6 and anti-NLRP3.

Transient transfection. Chemically-synthesized HDAC6 siRNA (h) targeting HDAC6 was purchased from Santa Cruz Biotechnology, Inc. U-87 MG cells were seeded in 6-well culture dishes with 2 ml antibiotic-free DMEM/F12 medium that was supplemented with FBS. The cells were incubated at 37˚C in a CO_2 incubator until the cells attained 30-50% confluency. The HDAC6 siRNA and control siRNA were diluted with siRNA transfection medium. The transfection reagent was also diluted in siRNA transfection medium. The mixture of siRNA and transfection reagent was incubated for 15-45 min at room temperature. For each transfection, 0.2 ml transfection mixture was added in 0.8 ml transfection medium. After washing the cells with 2 ml of transfection medium, the cells were transfected with HDAC6 siRNA (60 pmol) and control siRNA (60 pmol) for 7 h at 37˚C. Following incubation, 1 ml DMEM/F12 medium containing 2X normal serum and antibiotics concentration. was added to each well without the removal of the transfection mixture. The cells were then incubated for an additional 24 h. The medium was aspirated and replaced with fresh 1X normal growth medium. After 24 h, the HDAC6 level in U-87 MG cells were assessed using western blotting. Negative control siRNA was used for assessing nonspecific gene-silencing effects.

Statistical analysis. SPSS 21.0 statistics software (IBM Corp.) was used to perform all statistical analyses. One-way analysis of variance was used for determining differences in experimental groups followed by Tukey's test. Results of the behaviors tests are presented as mean ± SEM. Other experiment data is presented as mean ± SD unless otherwise stated. $P<0.05$ was considered to indicate a statistically significant difference.

Results

Morphological analysis and behavioral testing for CIBP rats. The establishment and assessment of CIBP rats followed the protocol as shown in Fig. 1A. In the present study, a rat model of CIBP was established by inoculating MRMT-1 cells into the medullary cavity of the tibia. Following two weeks of surgery, X-ray, histological analysis and behavioral testing verified the model. In contrast to the sham group, X-ray radiographs showed there to be bone damage and destruction in the tibias of CIBP rats (Fig. 1B). Tibial bone H&E staining demonstrated that trabecular bone was markedly destroyed in the CIBP rat compared with the sham group (Fig. 1C). Behavioral

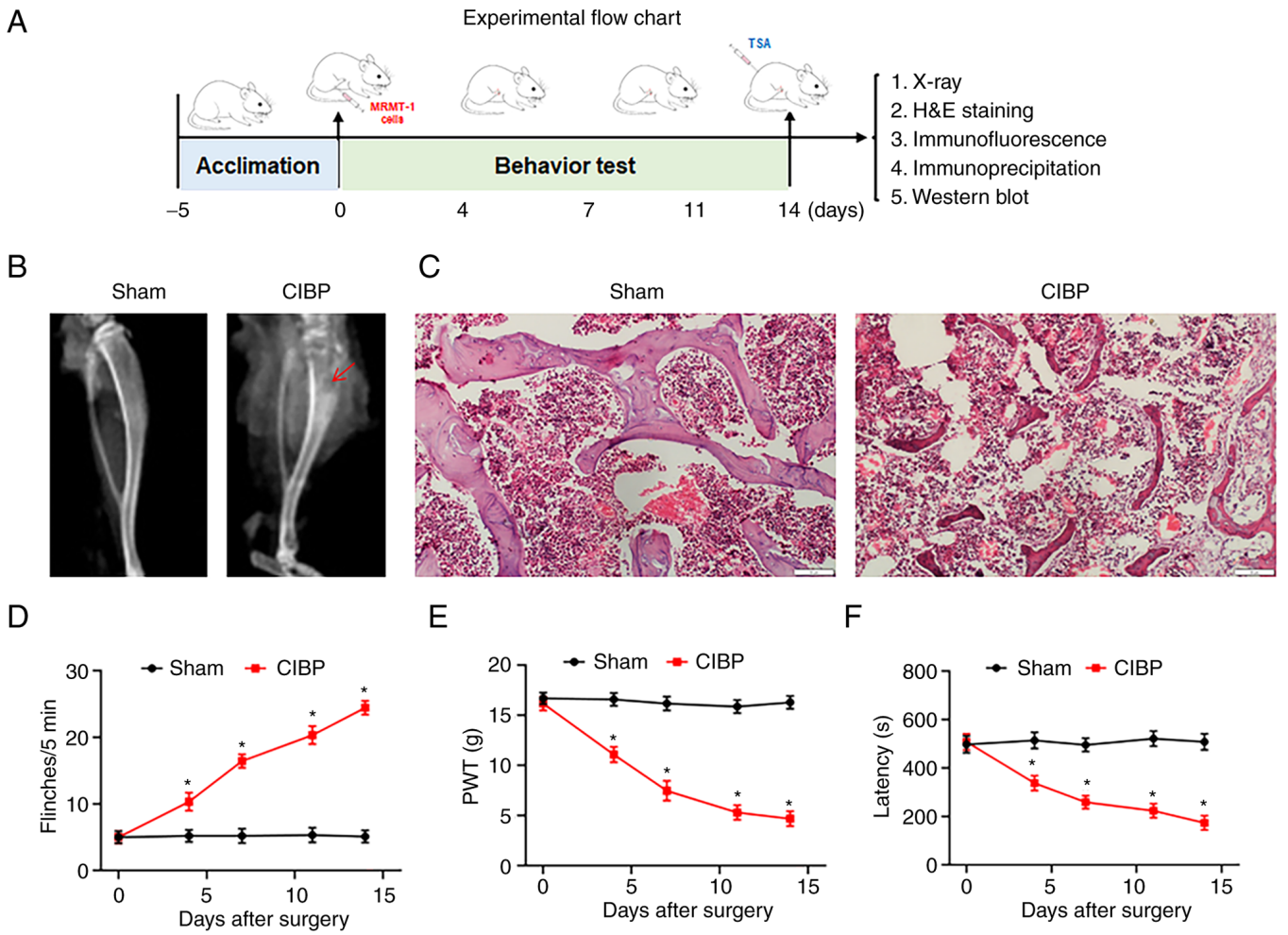

Figure 1. Validation of CIBP rat model. (A) Schematic diagram of the experimental procedures. On day 0, CIBP model was established. On day 0, 4, 7, 14 after surgery, the behavioral tests including spontaneous flinches record, PWT value test and latency to fall assay were performed. On day 14, X-ray scan, histology staining, western blotting, immunofluorescence assays were performed after behavioral tests. (B) Representative radiographs of the ipsilateral tibia from sham and CIBP rats on day 14. The red arrow indicated areas of bone destruction. n=9. (C) Representative images of hematoxylin and eosin staining of tibial sections from sham and CIBP rats. Scale bars, 50 μm; n=3. (D) The numbers of spontaneous flinches of sham and CIBP rats. (E) PWT values was assessed by von Frey filaments with the up-and-down method. (F) The latency to fall of accelerated rotarod motor test in sham and CIBP rats. Data were expressed as the mean ± SEM (n=9). *P<0.05 vs. sham group. CIBP, cancer-induced bone pain; PWT, paw withdrawal threshold.

tests were performed on day 4, 7, 11 and 14 after surgery as a means of confirming whether the inoculation of cancer cells resulted in the development of pain-related behaviors in CIBP rats. The CIBP rats exhibited an increase in the number of flinches, proving spontaneous pain (Fig. 1D). There was also a decrease in PWT values, indicating increased mechanical pain sensitivity (Fig. 1E) and a reduced latency to fall, representing impaired motor coordination (Fig. 1F).

TSA treatment inhibits HDAC6 and alleviates pain behaviors. As the inhibition of HDAC6 has an effect on neuropathic pain (39), immunofluorescence and western blot assays were applied in the present study for analyzing HDAC6 expression and phosphorylation in the spinal cord tissue. The phosphorylation of HDAC6 at serine 22 (pHDAC6-Ser22) increases HDAC6 deacetylase activity (40). The immunofluorescence images showed co-localization of HDC6 and GFAP in the spinal dorsal horn. Compared with the sham rats, HDAC6 and GFAP intensities increased in the spinal dorsal horn of CIBP rats. The increased fluorescence intensities in CIBP rats were reduced by TSA treatment (Fig. 2A and B). Western blot analysis found the level of pHDAC6-Ser22 in the spinal cord was upregulated in the CIBP group and decreased following TSA treatment (Fig. 2C and D). The behavioral tests were then performed. In contrast to the CIBP rats, following the intrathecal injection of TSA at 2, 4 and 6 h, the TSA-treated CIBP rats exhibited a decrease in the number of flinches (Fig. 2E), an increase in PWT values (Fig. 2F) and an elevated latency to fall (Fig. 2G). These results demonstrated that spontaneous pain and mechanical hyperalgesia were alleviated and motor coordination was recovered in CIBP rats by the administration of TSA.

TSA treatment suppresses spinal inflammatory response. Neuroinflammation in the spinal cord is associated with pain. H&E staining was used in the present study for the detection of leukocyte infiltration in spinal cord tissue. As shown in Fig. 3A, an extensive leukocytes filtration was observed in the spinal dorsal horns of CIBP rats (P<0.05 vs. sham group, Fig. 3A). The production of cytokines such as TNF-α

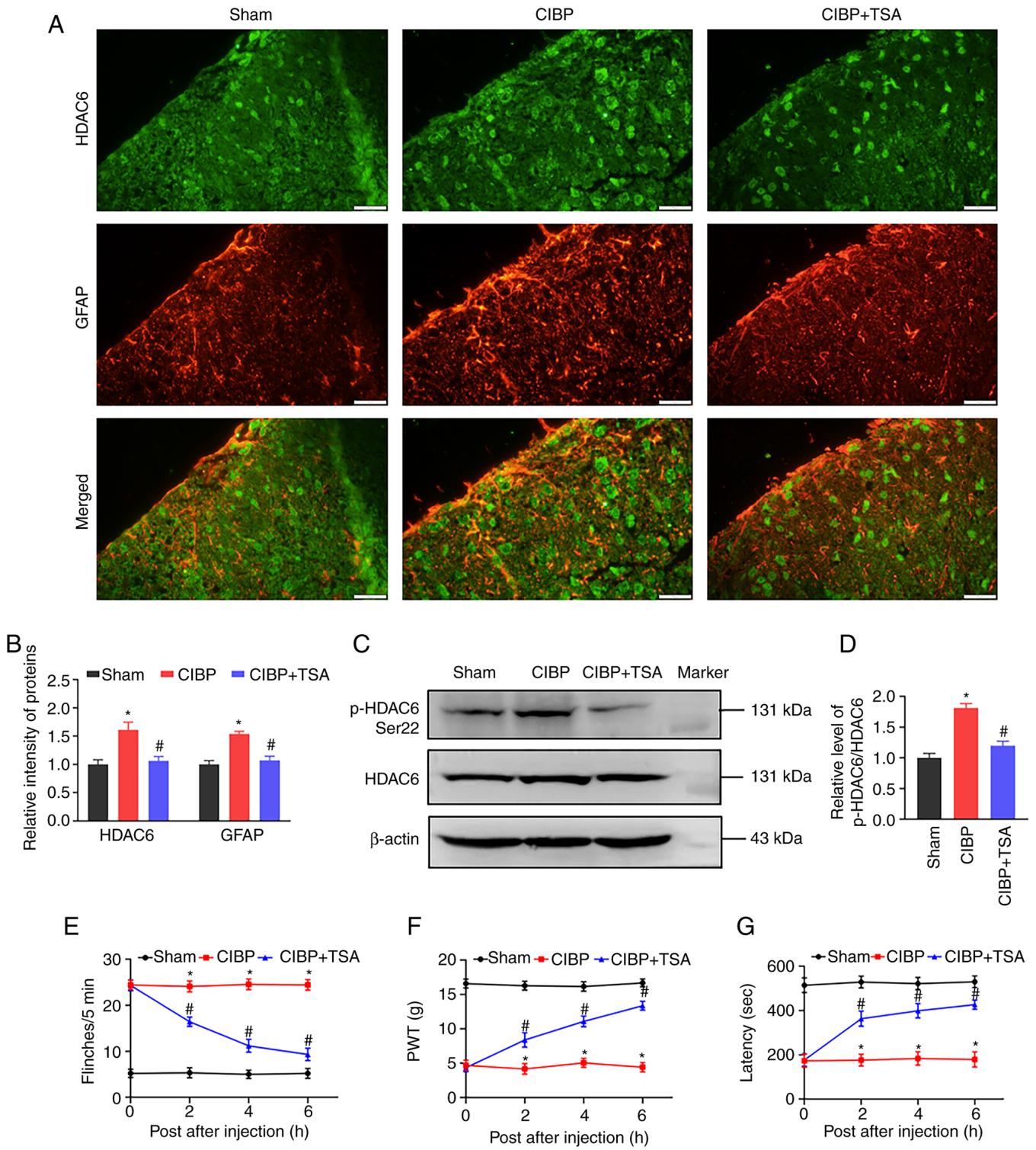

Figure 2. The effect of TSA on the spinal HDAC6 activation and behaviors tests. Representative immunofluorescence staining images (A) and quantitative analysis (B) for HDAC6 and GFAP in the spinal cord. Scale bar, 20 μm. Representative western blot bands (C) and quantitative analysis (D) of pHDAC6 (Ser22) protein in spinal cord. Data were presented as mean ± SD (n=3). *P<0.05 vs. sham group. $^{\#}$P<0.05 vs. CIBP group. Changes of numbers of spontaneous flinches (E), PWT values (F) and latency to fall (G) of rats after TSA treatment 2, 4 and 6 h. Data were expressed as the mean ± SEM (n=9). *P<0.05 vs. sham group. $^{\#}$P<0.05 vs. CIBP group. TSA, tubastatin A; HDAC6, histone deacetylase 6; GFAP, glial fibrillary acidic protein; CIBP, cancer-induced bone pain.

and IL-1β is involved in inflammatory response (41), so the immunofluorescence analysis of IL-1β intensity in the spinal dorsal horn was performed, the result showing IL-1β intensity to have robustly increased in the CIBP rats (P<0.05 vs. sham group; Fig. 3B). Similarly, western blot analysis showed IL-1β protein levels to be upregulated in the spinal cords of CIBP rats (P<0.05 vs. sham group; Fig. 3E and F). Following TSA treatment, the fluorescence intensity and protein levels of IL-1β were both reduced in the spinal cords (P<0.05 vs. CIBP group, Fig. 3B, D-F). In addition to IL-1β, another pro-inflammatory cytokine TNF-α was also examined. The increased expression of TNF-α expression in the CIBP rats was reduced by

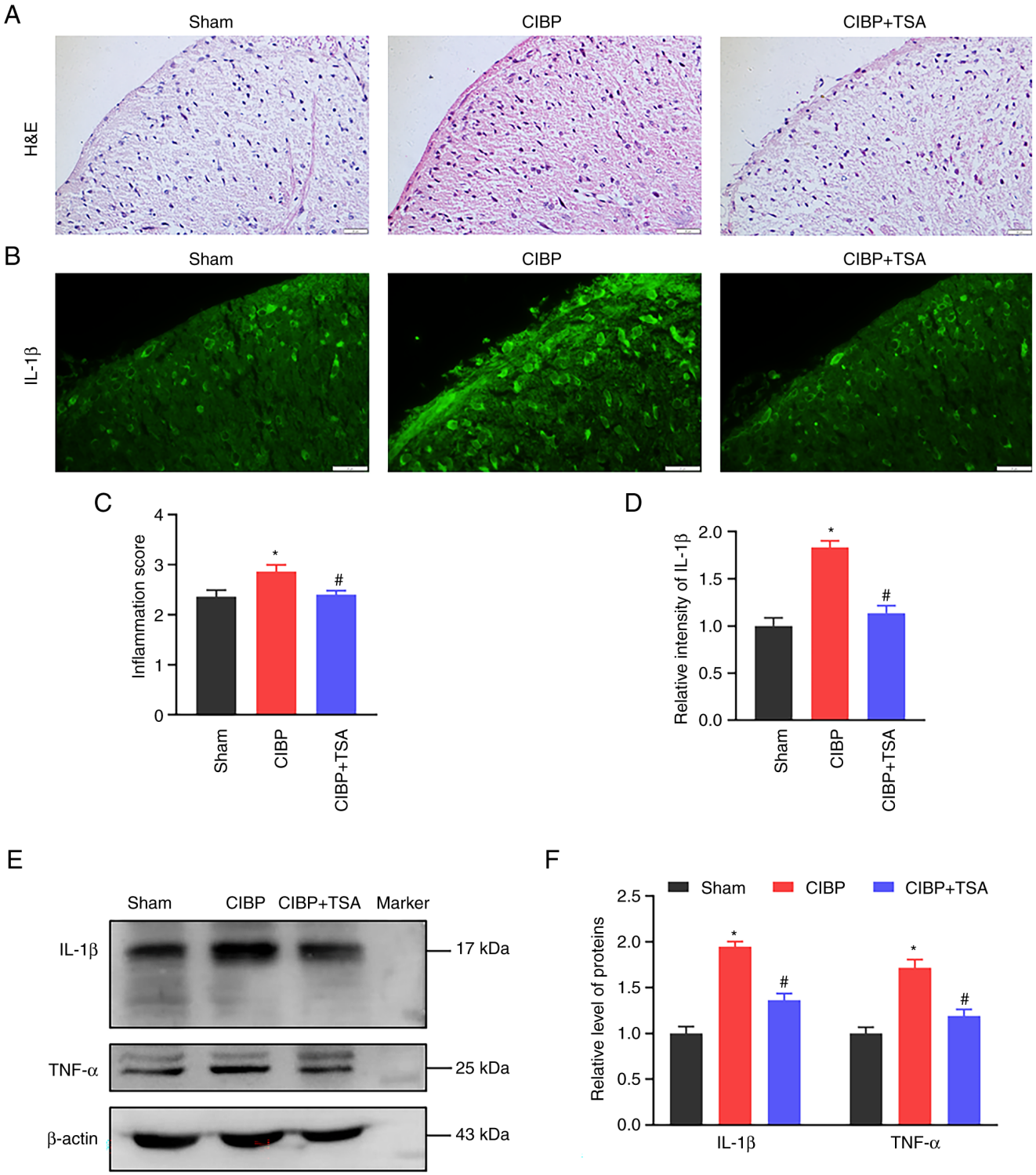

Figure 3. Effect of TSA on neuroinflammation in the spinal cord. Representative images (A) and quantitative analysis (C) of hematoxylin and eosin staining for spinal cord in sham, CIBP and CIBP + TSA group rats. Scale bar, 20 μm. Representative immunofluorescence staining images (B) and quantitative analysis (D) for IL-1β in spinal cord. Scale bar, 20 μm. Representative western blot bands (E) and quantitative analysis (F) of IL-1β and TNF-α protein in spinal cord in sham, CIBP and CIBP + TSA group rats. Data were presented as mean ± SD (n=3). *P<0.05 vs. sham group. #P<0.05 vs. CIBP group. TSA, tubastatin A; CIBP, cancer-induced bone pain.

TSA treatment (P<0.05 vs. CIBP group, Fig. 3E and F). These results suggest that TSA treatment decrease the production of inflammatory cytokines in the spinal cords of the CIBP rats.

TSA treatment reduces spinal astrocytic activation. Activated astrocyte promotes inflammatory cytokines releases, which includes IL-1β and TNF-α. GFAP is the hallmark intermediate filament protein that is found in astrocytes (42). CFB rapidly amplifies C3 activation (43), which is linked to astrocyte reactivity and the promotion of the neuroinflammatory phenotype (44). GFAP, C3 and CFB expression levels were detected in the present study. Immunofluorescence

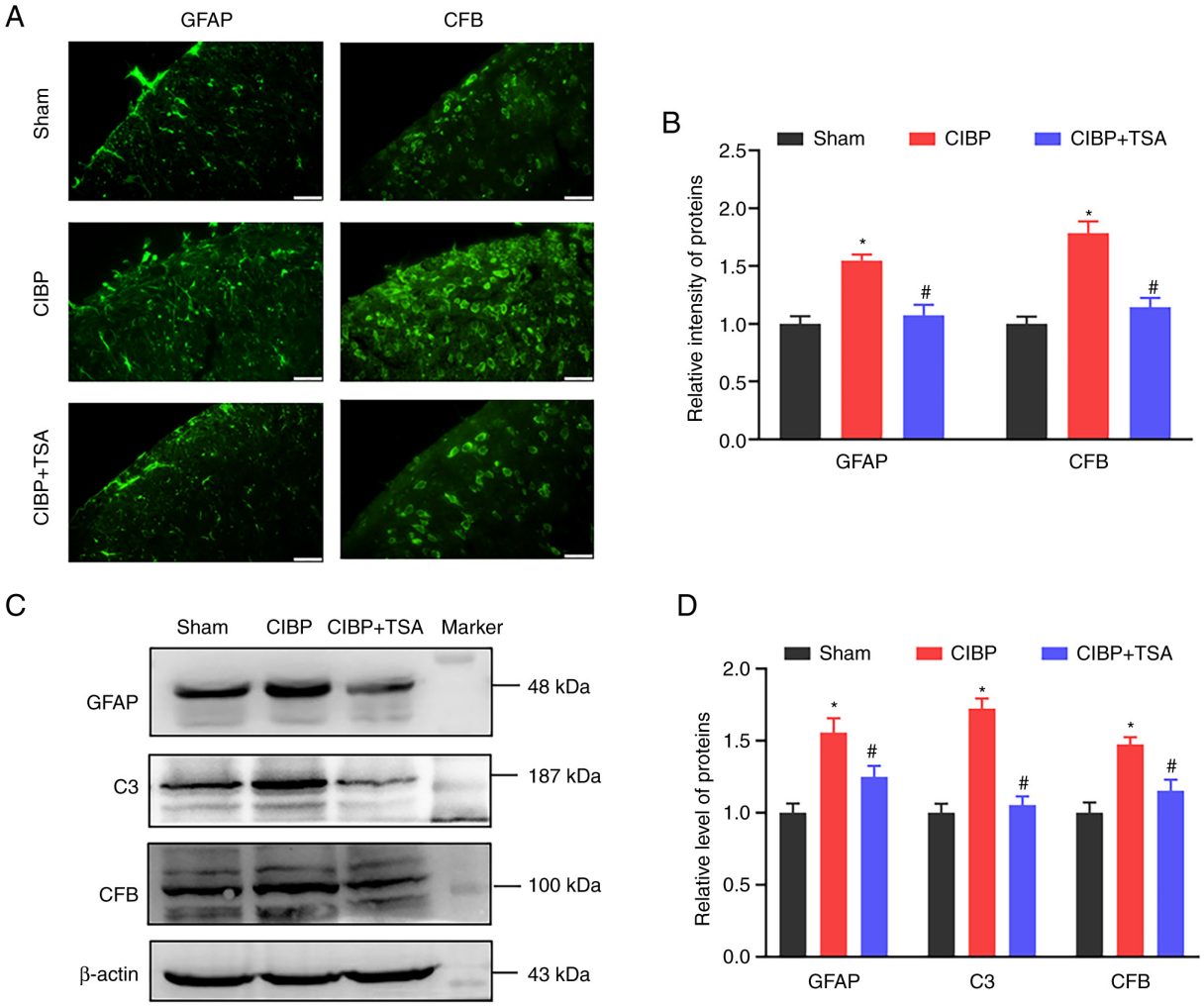

Figure 4. Effect of TSA on the spinal astrocytic activation. Representative immunofluorescence staining images (A) and quantitative analysis (B) for GFAP and CFB in the spinal cord. Scale bar, 20 μm. Representative western blot bands (C) and quantitative analysis (D) of GFAP, C3 and CFB proteins in the spinal cord. Data were presented as mean ± SD (n=3). *P<0.05 vs. sham group. #P<0.05 vs. CIBP group. TSA, tubastatin A; GFAP, glial fibrillary acidic protein; CFB, complement factor B; CIBP, cancer-induced bone pain.

images showed that the GFAP and CFB intensities in the spinal dorsal horn were significantly increased in the CIBP rats (P<0.05 vs. sham group) and reduced following TSA treatment (P<0.05 vs. CIBP group; Fig. 4A and B). Western blot analysis found the GFAP and CFB protein levels to be upregulated in the spinal cords of the CIBP rats, compared with the sham group (P<0.05 vs. sham group; Fig. 4C and D). Following TSA treatment, the upregulated levels of GFAP and CFB were reduced (P<0.05 vs. CIBP group; Fig. 4C and D). In addition, increased spinal C3 level were also detected in the CIBP rats (P<0.05 vs. sham group) and TSA treatment reduced C3 levels in the CIBP rats (P<0.05 vs. CIBP group; Fig. 4C and D). These results suggest that TSA treatment suppressed astrocytic activation in the spinal cords of the CIBP rats.

TAS treatment decreases NLRP3 inflammasome activation and NF-κB expression. As IL-1β maturation can be catalyzed by NLRP3 inflammasome activation, the effect of TSA on activation of NLRP3 inflammasome was further investigated. Immunofluorescence images showed the intensities of NLRP3 and caspase-1 to have increased in the spinal cords of the CIBP rats (P<0.05 vs. sham group) and TSA treatment reduced these upregulations (P<0.05 vs. CIBP group; Fig. 5A and B). Western blot analysis showed the components of NLRP3 inflammasome and cleaved caspase-1 protein levels to be upregulated in the spinal cords of the CIBP rats (P<0.05 vs. sham group; Fig. 5C and E). Similarly, TSA treatment downregulated the NLRP3 and cleaved caspase-1 expression levels in the CIBP rats (P<0.05 vs. CIBP group; Fig. 5C and E). To provide further confirmation of the interaction between NLRP3 and HDAC6, immunoprecipitation was performed. As can be seen in Fig. 5D, input represented a positive control for demonstrating the existence of HDAC6 and NLRP3 in the spinal cord tissue extracts. Immune complexes were obtained from tissue lysates following incubation with anti-HDAC6 or anti-NLRP3 antibodies. The presence of HDAC6 or NLRP3 proteins in the immunoprecipitants was measured by probing with anti-HDAC6 or anti-NLRP3 antibodies. The interaction between HDAC6 and NLRP3 was found to have increased in the spinal cords of the CIBP rats (P<0.05 vs. sham group) and TSA treatment reduced the association of HDAC6 to NLRP3 (P<0.05 vs. CIBP group; Fig. 5D and F). In addition to NLRP3 inflammasome, NF-κB also regulates the

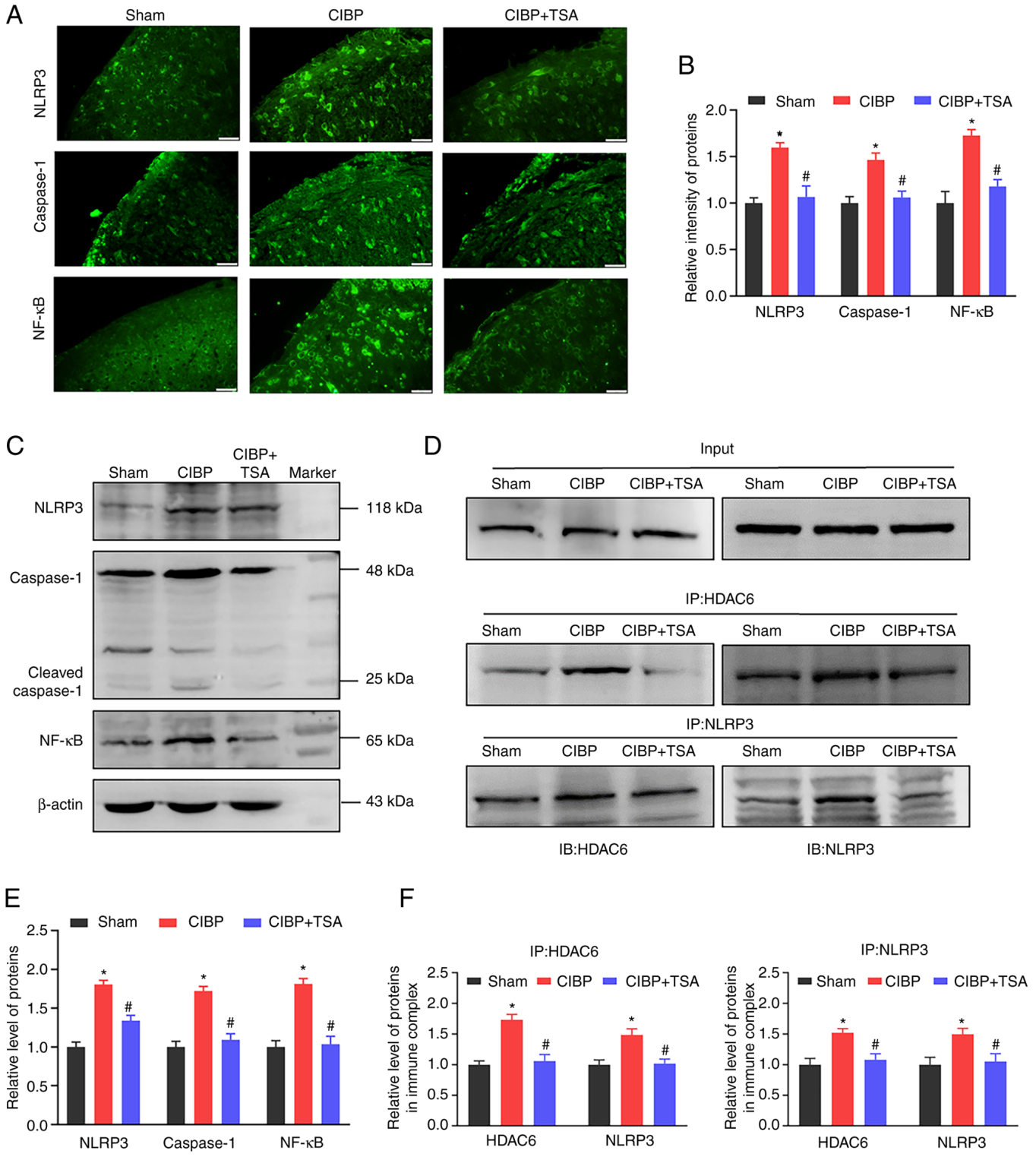

Figure 5. Effect of TSA on NLRP3 inflammasome activation and NF-κB. (A) Representative immunofluorescence staining images and (B) quantitative analysis for NLRP3, caspase-1 and NF-κB in the spinal cord. Scale bar, 20 μm. (C) Representative western blot bands and (E) quantitative analysis of NLRP3, caspase-1 and NF-κB proteins in spinal cord. (D and F) HDAC6 interaction with NLRP3 detected by immunoprecipitation assay. Spinal tissue lysates were immunoprecipitated with anti-HDAC6 and anti-NLRP3 antibodies and immunoblots were probed with anti-NLRP3 and anti-HDAC6 antibodies. The input panel showed target proteins prior to immunoprecipitation in the extracts. Data were presented as mean ± SD (n=3). *P<0.05 vs. sham group. #P<0.05 vs. CIBP group. TSA, tubastatin A; NLRP3, NOD-like receptor pyrin domain containing 3; HDAC6, histone deacetylase 6; CIBP, cancer-induced bone pain.

expression of pro-inflammatory cytokines. As Fig. 5A shows, NF-κB intensity was increased in the spinal dorsal horns of the CIBP rats (P<0.05 vs. sham group; Fig. 5A and B). Western blot analysis demonstrated that the NF-κB protein level was up-regulated in the spinal cords of the CIBP rats (P<0.05 vs. sham group; Fig. 5C and E). Following TSA treatment, the upregulated level of NF-κB was found to have reduced in the spinal cords of the CIBP rats (P<0.05 vs. CIBP

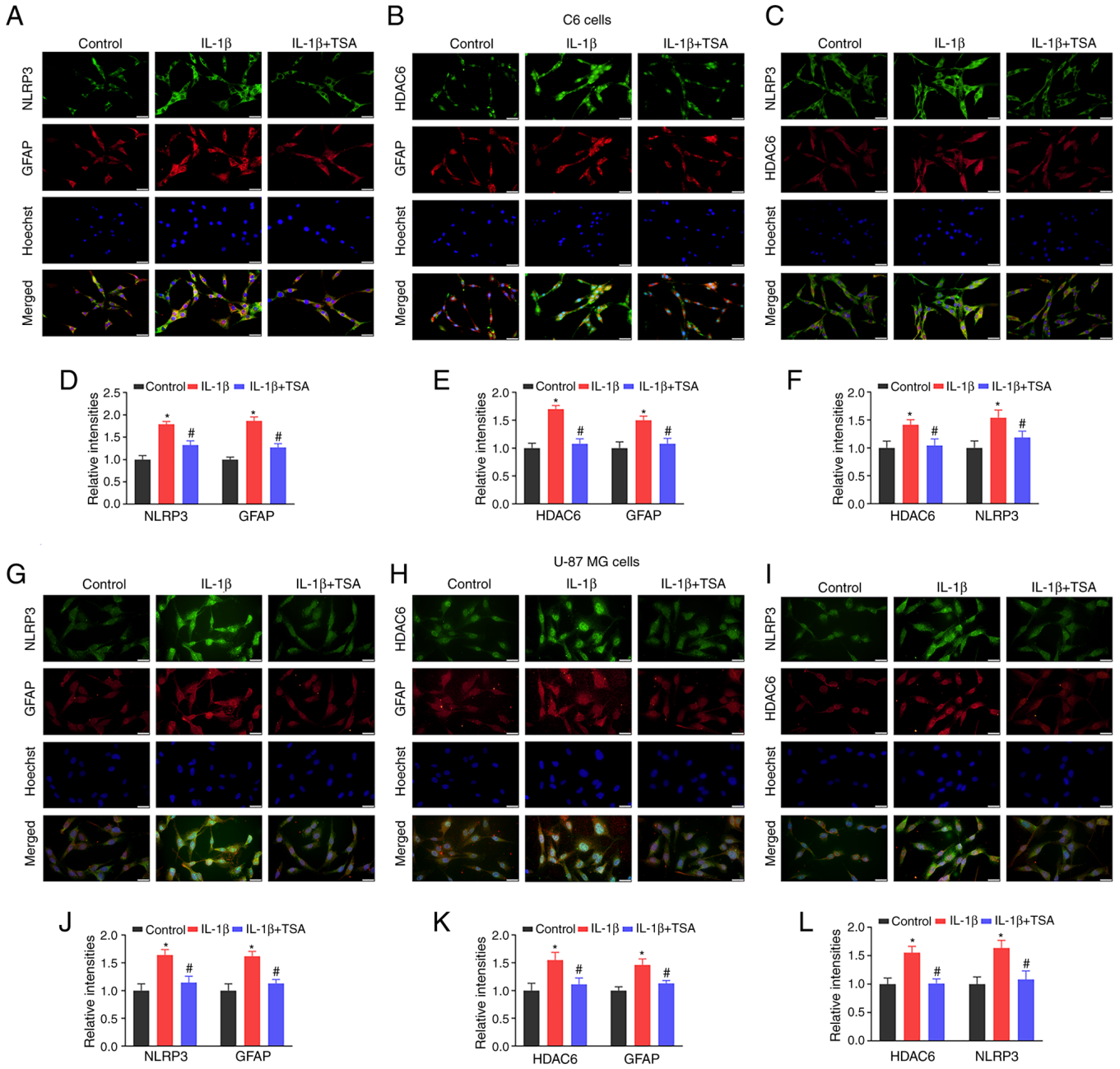

Figure 6. Effect of TSA on HDAC6 and NLRP3 expression in C6 and U-87 MG cells. (A-C and G-I) Representative immunofluorescence staining images and (D-F and J-L) quantitative analysis for NLRP3, HDAC6 and GFAP in C6 and U-87 MG cells. Cells were counterstained with Hoechst 33342 (blue). Scale bar, 20 μm; magnification, x60). Data were presented as mean ± SD (n=3). *P<0.05 vs. control group. $^{\#}$P<0.05 vs. IL-1β group. TSA, tubastatin A; HDAC6, histone deacetylase 6; NLRP3, NOD-like receptor pyrin domain containing 3.

group; Fig. 5C and E. These findings collectively indicated that TSA treatment suppressed the binding between HDAC6 and NLRP3, decreased NLRP3 inflammasome activation and reduced the expression of NF-κB.

TSA treatment reduces HDAC6 and NLRP3 expression in IL-1β-induced C6 and U-87 MG cells. As a means of further confirming that the effects of HDAC6 on NLRP3 were related to glial cell activation, the association and expression of HDAC6 and NLRP3 in IL-1β-induced C6 and U-87 MG cells after TSA treatment was investigated. Double-label immunofluorescence staining found a colocalization of HDA6 and NLRP3 in glial cells. As can be seen in Fig. 6, NLRP3 and HDAC6 were colocalized with astrocyte marker GFAP in both C6 and U-87 MG cells. Compared with the control group, HDAC6, NLRP3 and GFAP fluorescence intensities were all increased in IL-1β-induced C6 and U-87 MG cells (P<0.05; Fig. 6). Following TSA treatment, the HDAC6, NLRP3 and GFAP intensities were reduced, compared with the IL-1β group (P<0.05, Fig. 6). These results demonstrated that TSA treatment decreased NLRP3 inflammasome activation in glial cells.

In order to verify the effect of HDAC6 expression has on the changes in NLRP3 expression and inflammatory factor, HDAC6 siRNA was used for treating U-87 cells. As Fig. 7 shows, HDAC6 siRNA reduced NLRP3 and downstream

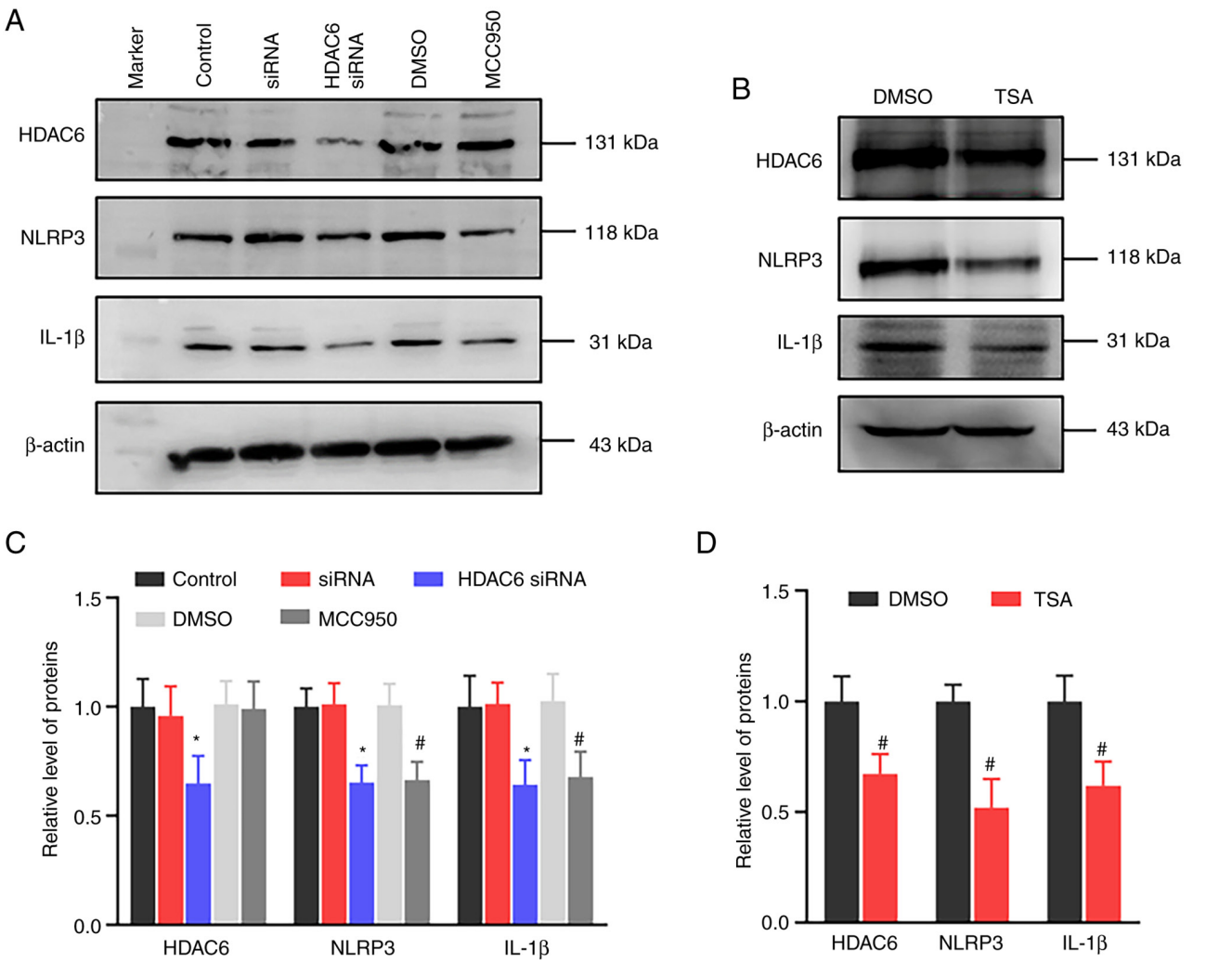

Figure 7. Effects of HDAC6 siRNA, MCC950 and TSA on the NLRP3 and IL-1β expression in U-87 MG cells. (A and B) Western blotting measured the protein levels of HDAC6, NLRP3 and IL-1β in U-87 MG cells transfected with HDAC6 siRNA or treated with MCC950 or treated with TSA. (C and D) Relative protein levels in (A and B) are expressed as fold changes over control. Data were presented as mean ± SD (n=3). *P<0.05 vs. siRNA group. #P<0.05 vs. DMSO group. HDAC6, histone deacetylase 6; si, short interfering; TSA, tubastatin A; NLRP3, NOD-like receptor pyrin domain containing 3.

inflammatory factor IL-1β expressions. Similarly, the NLRP3 inhibitor MCC950 and treatment also decreased NLRP3 and IL-1β expressions. In addition, TSA-treated U-87 MG cells showed decreased NLRP3 and HDAC6 expressions. The results indicated that the downregulation of HDAC6 had an inhibitory effect on the NLRP3-mediated inflammatory factor expression.

Discussion

Neuroinflammation of the spinal cord is an important mechanism for cancer-induced bone pain generation and maintenance (7-9). A CIBP rat model was established in the present study and increased pain sensitivity and impaired motor ability were observed in the CIBP rats. The present study focused on the effect HDAC6 has on pain and spinal inflammation. TSA is a potent and selective HDAC6 inhibitor that has been reported to have an inhibitory effect on inflammatory response and pain management. TSA treatment results in reduced IL-6 expression and mediated inflammatory response while also eliciting anti-inflammatory and antirheumatic effects in Freund's complete adjuvant-induced inflammation mouse model and collagen-induced arthritis mouse model (45). The intravenous administration of TSA also inhibits HDAC6 activity and limits NLRP3 inflammasome activation and cell pyroptosis in the ischemia/reperfusion injury model (46). At the same time, TSA treatment has been found to increase mu-opioid receptor expression, ameliorate tactile hypersensitivity and enhance the analgesic effect of morphine in the bone cancer pain rat model (33). TSA treatment decreased IL-1β and TNF-α expressions and inflammatory infiltration in the spinal cords of the CIBP rats in the present study. Based on the aforementioned studies, it can be seen that the analgesic effect of TSA contributed to the inhibition of spinal inflammation.

The mechanisms of pain that are induced in patients with bone metastasis include inflammatory and neuropathic processes. In the present study, increased infiltration of inflammatory cells and IL-1β expression were observed in the spinal dorsal horns of the CIBP rats. These changes were involved in the inflammatory processes. In addition, the relationship between neuroinflammation and pain behaviors was measured

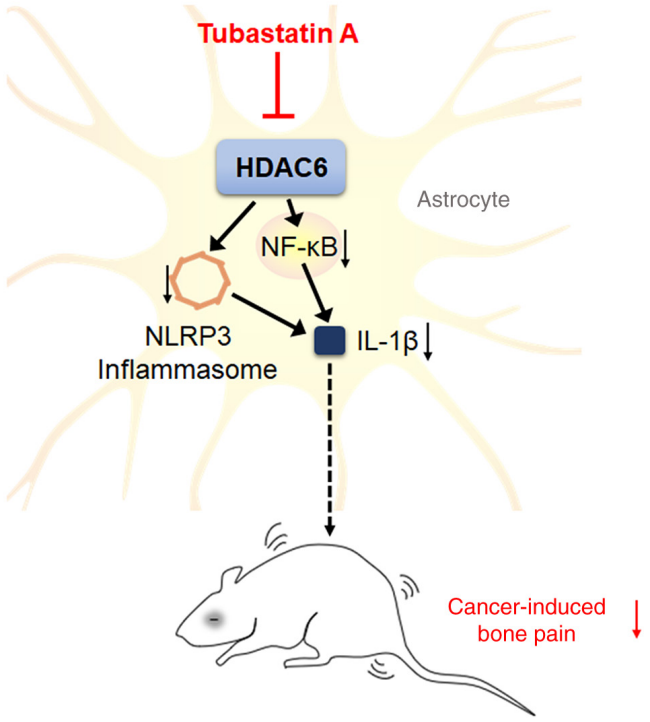

Figure 8. Schematic representation of TSA treatment attenuates pain behaviors in CIBP rats through inhibiting HDAC6 activity and consequently reducing inflammatory response. TSA, tubastatin A; CIBP, cancer-induced bone pain; HDAC6, histone deacetylase 6; NLRP3, NOD-like receptor pyrin domain containing 3.

(Fig. 3). The present study and previous research have shown that the inflammatory signal increases in the spinal cords of CIBP animals, which is accompanied by hyperalgesia and pharmacologic inhibition of inflammatory factors expression and that the inflammatory response could serve to alleviate pain behaviors (47,48). In the spinal cord, the inflammation factor is mainly derived from microglia and astrocytes. The reason that astrocytes were chosen in the present study is because astrocytic reaction is more persistent, in both animal models of inflammatory pain and neuropathic pain, compared with microglia reaction (49). Cancer-induced bone pain is a type of chronic pain in which both inflammatory and neuropathic factors are involved. Research on microglia has further indicated that microgliosis is not always associated with pain states and neuropathic pain can be reduced without any microgliosis changes occurring (50). Accordingly, spinal astrocytes play an important role in chronic pain maintenance. In addition, the inhibition of GFAP (astrocytic marker) expression and astrogliosis is associated with a reduction in neuropathic pain behaviors rather than microglial reaction. The intrathecal knockdown of GFAP expression in nerve-injured animals also reduces neuropathic pain behaviors (51).

Studies have indicated that HDAC6 is responsible for the regulation of NLRP3 inflammasome activation and the expression of pro-inflammatory cytokines. First, HDAC6 directly binds with NLRP3 through its ubiquitin-binding domain (52). Second, HDAC6 works as a dynein adapter and facilitates the assembly of NLRP3 inflammasome. HDAC6 deacetylates α-tubulin through its deacetylase domain and promotes NLRP3 inflammasome assembly (27). The inhibition of HDAC6 deacetylase activity by tubastatin A, rocilinostat and tubacin increases α-tubulin acetylation while also blocking the activation of NLRP3 inflammasome (29). Third, HDAC6 regulates the NF-κB-mediated expression of pro-inflammatory cytokines. HDAC6 deacetylates the p65 subunit of NF-κB and decreases its DNA-binding activity (53), which reduces inflammatory gene expression that includes NLRP3, pro-IL-1β and pro-IL-18 as a consequence (54). In the present study, NLRP3 inflammasome activation was observed in the CIBP rats and was found to be inhibited by TSA treatment. TSA treatment decreased spinal inflammation via HDAC6/NLRP3 and NF-κB signaling.

In summary, elevated pain sensitivity, spinal astrocyte activation and increased neuroinflammatory response were all found in the CIBP rats. TSA treatment was found to inhibit HDAC6 activity and reduce NLRP3 and NF-κB mediated inflammatory response, which consequently causes the alleviation of cancer pain (Fig. 8). Although the present study on cancer-induced bone pain rats provided possibilities and potential target for analgesia, there are still some limitations to it. First, in the present study, CIBP model was established by intratibial inoculation of cancer cells. Elsewhere, intracardiac inoculation is also commonly used. Upon intracardiac inoculation, most substantial bone destruction tends to occur in the metaphyses of the distal femur and proximal tibia. Intratibial inoculation is used when a study focusses on the changes following bone metastasis (55). Detecting the effect of TSA on different CIBP models is helpful for the application of TSA on pain management. Second, in the present study, HDAC6 was considered as the target protein for CIBP management. However, the expression of HDAC6 on the genetic level in animals was not constructed and needed further study.

Acknowledgements

Not applicable.

Funding

The present study was supported by the grants from the National Natural Science Foundation of China (grant nos. 81971066 and 32100823), Research Project of Science and Technology Department of Hubei Province of China (grant nos. 2022CFB356, 2022CFB791 and 2022SFYF014).

Availability of data and materials

The datasets generated and analyzed during the present study are available from the corresponding author on reasonable request.

Authors' contributions

All authors made a significant contribution to the present study. MX and LL conceived and designed the study. YH, ZW and YY performed the experiments, DL, SZ, JD, WM and HZ collected and analyzed the data. MX and LL drafted and edited the manuscript. YH, ZW and YY confirm the authenticity of all the raw data. All authors read and approved the final manuscript.

Ethics approval and consent to participate

The present study was approved by the Ethics Committee of Hubei University of Science and Technology (approval number 2020-01-900). All experimental procedures in the present study were complied with the local and international guidelines on ethical use of animals.

Patient consent for publication

Not applicable.

Competing interests

The authors declare that they have no competing interests.

References

1. Yang J, Wahner-Roedler DL, Zhou X, Johnson LA, Do A, Pachman DR, Chon TY, Salinas M, Millstine D and Bauer BA: Acupuncture for palliative cancer pain management: Systematic review. BMJ Support Palliat Care 11: 264-270, 2021.
2. Jiang W, Rixiati Y, Zhao B, Li Y, Tang C and Liu J: Incidence, prevalence and outcomes of systemic malignancy with bone metastases. J Orthop Surg (Hong Kong) 28: 2309499020915989, 2020.
3. Fornetti J, Welm AL and Stewart SA: Understanding the bone in cancer metastasis. J Bone Miner Res 33: 2099-2113, 2018.
4. Coleman RE, Croucher PI, Padhani AR, Clézardin P, Chow E, Fallon M, Guise T, Colangeli S, Capanna R and Costa L: Bone metastases. Nat Rev Dis Primers 6: 83, 2020.
5. Pfister DG, Spencer S, Adelstein D, Adkins D, Anzai Y, Brizel DM, Bruce JY, Busse PM, Caudell JJ, Cmelak AJ, *et al*: Head and neck cancers, version 2.2020, NCCN clinical practice guidelines in oncology. J Natl Compr Canc Netw 18: 873-898, 2020.
6. Brozović G, Lesar N, Janev D, Bošnjak T and Muhaxhiri B: Cancer pain and therapy. Acta Clin Croat 61 (Suppl 2): S103-S108, 2022.
7. Gallaway MS, Townsend JS, Shelby D and Puckett MC: Pain among cancer survivors. Prev Chronic Dis 17: E54, 2020.
8. Falk S and Dickenson AH: Pain and nociception: Mechanisms of cancer-induced bone pain. J Clin Oncol 32: 1647-1654, 2014.
9. Yam MF, Loh YC, Tan CS, Khadijah Adam S, Abdul Manan N and Basir R: General pathways of pain sensation and the major neurotransmitters involved in pain regulation. Int J Mol Sci 19: 2164, 2018.
10. Zheng XQ, Wu YH, Huang JF and Wu AM: Neurophysiological mechanisms of cancer-induced bone pain. J Adv Res 35: 117-127, 2021.
11. Shi Y, Gelman BB, Lisinicchia JG and Tang SJ: Chronic-pain-associated astrocytic reaction in the spinal cord dorsal horn of human immunodeficiency virus-infected patients. J Neurosci 32: 10833-10840, 2012.
12. Göbel A, Dell'Endice S, Jaschke N, Pählig S, Shahid A, Hofbauer LC and Rachner TD: The role of inflammation in breast and prostate cancer metastasis to bone. Int J Mol Sci 22: 5078, 2021.
13. Shupp AB, Kolb AD, Mukhopadhyay D and Bussard KM: Cancer metastases to bone: Concepts, mechanisms and interactions with bone osteoblasts. Cancers (Basel) 10: 182, 2018.
14. Chen R, Yin C, Fang J and Liu B: The NLRP3 inflammasome: An emerging therapeutic target for chronic pain. J Neuroinflammation 18: 84, 2021.
15. Moossavi M, Parsamanesh N, Bahrami A, Atkin SL and Sahebkar A: Role of the NLRP3 inflammasome in cancer. Mol Cancer 17: 158, 2018.
16. Zhang YZ, Zhang YL, Huang Q, Huang C, Jiang ZL, Cai F and Shen JF: AdipoRon alleviates free fatty acid-induced myocardial cell injury via suppressing Nlrp3 inflammasome activation. Diabetes Metab Syndr Obes 12: 2165-2179, 2019.
17. D'Amico R, Fusco R, Siracusa R, Impellizzeri D, Peritore AF, Gugliandolo E, Interdonato L, Sforza AM, Crupi R, Cuzzocrea S, *et al*: Inhibition of P2X7 purinergic receptor ameliorates fibromyalgia syndrome by suppressing NLRP3 pathway. Int J Mol Sci 22: 6471, 2021.
18. Corcoran SE, Halai R and Cooper MA: Pharmacological inhibition of the Nod-like receptor family pyrin domain containing 3 inflammasome with MCC950. Pharmacol Rev 73: 968-1000, 2021.
19. Chen SP, Zhou YQ, Wang XM, Sun J, Cao F, HaiSam S, Ye DW and Tian YK: Pharmacological inhibition of the NLRP3 inflammasome as a potential target for cancer-induced bone pain. Pharmacol Res 147: 104339, 2019.
20. Starobova H, Monteleone M, Adolphe C, Batoon L, Sandrock CJ, Tay B, Deuis JR, Smith AV, Mueller A, Nadar EI, *et al*: Vincristine-induced peripheral neuropathy is driven by canonical NLRP3 activation and IL-1β release. J Exp Med 218: e20201452, 2021.
21. Seidel C, Schnekenburger M, Dicato M and Diederich M: Histone deacetylase 6 in health and disease. Epigenomics 7: 103-118, 2015.
22. English K and Barton MC: HDAC6: A key link between mitochondria and development of peripheral neuropathy. Front Mol Neurosci 14: 684714, 2021.
23. Shen S, Picci C, Ustinova K, Benoy V, Kutil Z, Zhang G, Tavares MT, Pavlíček J, Zimprich CA, *et al*: Tetrahydroquinoline-capped histone deacetylase 6 inhibitor SW-101 ameliorates pathological phenotypes in a charcot-marie-tooth type 2A mouse model. J Med Chem 64: 4810-4840, 2021.
24. Van Helleputte L, Kater M, Cook DP, Eykens C, Rossaert E, Haeck W, Jaspers T, Geens N, Vanden Berghe P, Gysemans C, *et al*: Inhibition of histone deacetylase 6 (HDAC6) protects against vincristine-induced peripheral neuropathies and inhibits tumor growth. Neurobiol Dis 111: 59-69, 2018.
25. Krukowski K, Ma J, Golonzhka O, Laumet GO, Gutti T, van Duzer JH, Mazitschek R, Jarpe MB, Heijnen CJ and Kavelaars A: HDAC6 inhibition effectively reverses chemotherapy-induced peripheral neuropathy. Pain 158: 1126-1137, 2017.
26. Prior R, Van Helleputte L, Klingl YE and Van Den Bosch L: HDAC6 as a potential therapeutic target for peripheral nerve disorders. Expert Opin Ther Targets 22: 993-1007, 2018.
27. Chang P, Li H, Hu H, Li Y and Wang T: The role of HDAC6 in autophagy and NLRP3 inflammasome. Front Immunol 12: 763831, 2021.
28. Yan S, Wei X, Jian W, Qin Y, Liu J, Zhu S, Jiang F, Lou H and Zhang B: Pharmacological inhibition of HDAC6 attenuates NLRP3 inflammatory response and protects dopaminergic neurons in experimental models of parkinson's disease. Front Aging Neurosci 12: 78, 2020.
29. Magupalli VG, Negro R, Tian Y, Hauenstein AV, Di Caprio G, Skillern W, Deng Q, Orning P, Alam HB, Maliga Z, *et al*: HDAC6 mediates an aggresome-like mechanism for NLRP3 and pyrin inflammasome activation. Science 369: eaas8995, 2020.
30. Wu X, Zhang H, Qi W, Zhang Y, Li J, Li Z, Lin Y, Bai X, Liu X, Chen X, *et al*: Nicotine promotes atherosclerosis via ROS-NLRP3-mediated endothelial cell pyroptosis. Cell Death Dis 9: 171, 2018.
31. Godena VK, Brookes-Hocking N, Moller A, Shaw G, Oswald M, Sancho RM, Miller CC, Whitworth AJ and De Vos KJ: Increasing microtubule acetylation rescues axonal transport and locomotor deficits caused by LRRK2 Roc-COR domain mutations. Nat Commun 5: 5245, 2014.
32. Yao FD, Yang JQ, Huang YC, Luo MP, Yang WJ, Zhang B and Liu XJ: Antinociceptive effects of ginsenoside Rb1 in a rat model of cancer-induced bone pain. Exp Ther Med 17: 3859-3866, 2019.
33. Hou X, Weng Y, Ouyang B, Ding Z, Song Z, Zou W, Huang C and Guo Q: HDAC inhibitor TSA ameliorates mechanical hypersensitivity and potentiates analgesic effect of morphine in a rat model of bone cancer pain by restoring μ-opioid receptor in spinal cord. Brain Res 1669: 97-105, 2017.
34. Liu M, Cheng X, Yan H, Chen J, Liu C and Chen Z: MiR-135-5p alleviates bone cancer pain by regulating astrocyte-mediated neuroinflammation in spinal cord through JAK2/STAT3 signaling pathway. Mol Neurobiol 58: 4802-4815, 2021.
35. Dixon WJ: Efficient analysis of experimental observations. Annu Rev Pharmacol Toxicol 20: 441-62, 1980.
36. Shi X, Bai H, Wang J, Wang J, Huang L, He M, Zheng X, Duan Z, Chen D, Zhang J, *et al*: Behavioral assessment of sensory, motor, emotion and cognition in rodent models of intracerebral hemorrhage. Front Neurol 12: 667511, 2021.
37. Song ZP, Xiong BR, Guan XH, Cao F, Manyande A, Zhou YQ, Zheng H and Tian YK: Minocycline attenuates bone cancer pain in rats by inhibiting NF-κB in spinal astrocytes. Acta Pharmacol Sin 37: 753-762, 2016.

38. Song S, Guo R, Mehmood A, Zhang L, Yin B, Yuan C, Zhang H, Guo L and Li B: Liraglutide attenuate central nervous inflammation and demyelination through AMPK and pyroptosis-related NLRP3 pathway. CNS Neurosci Ther 28: 422-434, 2022.
39. Chen C, Liu A, Lu Q, Luo L, Li J, Ke J, Liu Y and Feng X: HDAC6 inhibitor ACY-1215 improves neuropathic pain and its comorbidities in rats of peripheral nerve injury by regulating neuroinflammation. Chem Biol Interact 353: 109803, 2022.
40. Mazzetti S, De Leonardis M, Gagliardi G, Calogero AM, Basellini MJ, Madaschi L, Costa I, Cacciatore F, Spinello S, Bramerio M, *et al*: Phospho-HDAC6 gathers into protein aggregates in parkinson's disease and atypical parkinsonisms. Front Neurosci 14: 624, 2020.
41. Dong ZB, Wang YJ, Wan WJ, Wu J, Wang BJ, Zhu HL, Xie M and Liu L: Resveratrol ameliorates oxaliplatin-induced neuropathic pain via anti-inflammatory effects in rats. Exp Ther Med 24: 586, 2022.
42. Hol EM and Pekny M: Glial fibrillary acidic protein (GFAP) and the astrocyte intermediate filament system in diseases of the central nervous system. Curr Opin Cell Biol 32: 121-130, 2015.
43. Vallee KJ and Fields JA: Caloric restriction mimetic 2-deoxyglucose reduces inflammatory signaling in human astrocytes: Implications for therapeutic strategies targeting neurodegenerative diseases. Brain Sci 12: 308, 2022.
44. Gharagozloo M, Smith MD, Jin J, Garton T, Taylor M, Chao A, Meyers K, Kornberg MD, Zack DJ, Ohayon J, *et al*: Complement component 3 from astrocytes mediates retinal ganglion cell loss during neuroinflammation. Acta Neuropathol 142: 899-915, 2021.
45. Mao Y, Zhou J, Liu X, Gu E, Zhang Z and Tao W: Comparison of different histone deacetylase inhibitors in attenuating inflammatory pain in rats. Pain Res Manag 2019: 1648919, 2019.
46. Xu J, Zhao X, Jiang X, He L, Wu X, Wang J, Chen Q, Li Y and Zhang M: Tubastatin A Improves post-resuscitation myocardial dysfunction by inhibiting NLRP3-mediated pyroptosis through enhancing transcription factor EB signaling. J Am Heart Assoc 11: e024205, 2022.
47. Zhao J, Yan Y, Zhen S, Yu L, Ding J, Tang Q, Liu L, Zhu H and Xie M: LY294002 alleviates bone cancer pain by reducing mitochondrial dysfunction and the inflammatory response. Int J Mol Med 51: 42, 2023.
48. Chen J, Cong X, Zhan X, Zhou Z and Zheng W: Effects of parecoxib on pain threshold and inflammatory factors IL-1β, IL-6 and TNF-α in spinal cord of rats with bone cancer pain. J Coll Physicians Surg Pak 29: 528-531, 2019.
49. Ji RR, Berta T and Nedergaard M: Glia and pain: Is chronic pain a gliopathy? Pain 154 (Suppl 1): S10-S28, 2013.
50. Chen G, Zhang YQ, Qadri YJ, Serhan CN and Ji RR: Microglia in pain: Detrimental and Protective roles in pathogenesis and resolution of pain. Neuron 100: 1292-1311, 2018.
51. Ji RR, Donnelly CR and Nedergaard M: Astrocytes in chronic pain and itch. Nat Rev Neurosci 20: 667-685, 2019.
52. Hwang I, Lee E, Jeon SA and Yu JW: Histone deacetylase 6 negatively regulates NLRP3 inflammasome activation. Biochem Biophys Res Commun 467: 973-8, 2015.
53. Yang CJ, Liu YP, Dai HY, Shiue YL, Tsai CJ, Huang MS and Yeh YT: Nuclear HDAC6 inhibits invasion by suppressing NF-κB/MMP2 and is inversely associated with metastasis of non-small cell lung cancer. Oncotarget 6: 30263-30276, 2015.
54. Barter MJ, Butcher A, Wang H, Tsompani D, Galler M, Rumsby EL, Culley KL, Clark IM and Young DA: HDAC6 regulates NF-κB signalling to control chondrocyte IL-1-induced MMP and inflammatory gene expression. Sci Rep 12: 6640, 2022.
55. Wright LE, Ottewell PD, Rucci N, Peyruchaud O, Pagnotti GM, Chiechi A, Buijs JT and Sterling JA: Murine models of breast cancer bone metastasis. Bonekey Rep 5: 804, 2016.

Copyright © 2023 Hu et al. This work is licensed under a Creative Commons Attribution-NonCommercial-NoDerivatives 4.0 International (CC BY-NC-ND 4.0) License.